NASA TECHNICAL NOTE

NASA TN D-4471

c. 1

NASA TN D-4471

EXPERIMENTAL STUDY OF AEROELASTIC INSTABILITY OF OVEREXPANDED ROCKET NOZZLE EXTENSIONS

by W. J. Tuovila and Norman S. Land

Langley Research Center
Langley Station, Hampton, Va.

NATIONAL AERONAUTICS AND SPACE ADMINISTRATION • WASHINGTON, D. C. • APRIL 1968

NASA TN D-4471

EXPERIMENTAL STUDY OF AEROELASTIC INSTABILITY OF OVEREXPANDED ROCKET NOZZLE EXTENSIONS

By W. J. Tuovila and Norman S. Land

Langley Research Center
Langley Station, Hampton, Va.

NATIONAL AERONAUTICS AND SPACE ADMINISTRATION

For sale by the Clearinghouse for Federal Scientific and Technical Information
Springfield, Virginia 22151 – CFSTI price $3.00

EXPERIMENTAL STUDY OF AEROELASTIC INSTABILITY OF OVEREXPANDED ROCKET NOZZLE EXTENSIONS

By W. J. Tuovila and Norman S. Land
Langley Research Center

SUMMARY

A brief exploratory investigation was conducted to study possible aeroelastic-instability phenomena which might occur for overexpanded flow through flexible nozzle extensions which are being considered for use in increasing the thrust of rocket engines at very high altitudes. Five conical extensions with a 22.5° half-angle and area ratios of 54 and 100 were fabricated from varying thicknesses of steel and glass-fiber laminates. Studies were conducted at constant stagnation pressure. Flow through the nozzle and extension started in an underexpanded condition but gradually changed to an overexpanded condition as the quiescent-flow ambient pressure increased. Two rigid aluminum-alloy models with geometry similar to that of the flexible models were used for pressure measurements and for visualization of flow across the exit and interior surface.

For some flexible extensions, dynamic instability was observed which could be related by means of flow measurements to an overexpanded flow condition that caused buckling loads. The experimental data are summarized graphically to indicate nozzle-extension parameters in the stable region for different loading conditions. The data may be useful as a guide for the preliminary design of nozzle extensions.

INTRODUCTION

A rocket nozzle operating over a range of altitudes will produce a maximum thrust at only one altitude if the area ratio is fixed. At altitudes above that for maximum thrust an improvement in nozzle efficiency may be obtained by adding an extension to increase the area ratio (ref. 1). Such extensions could be lightweight for operation in an underexpanded condition (exit static pressure greater than ambient pressure). Under off-design conditions, however, overexpansion could occur, with attendant collapsing loads and aeroelastic instabilities. This condition could occur for a short time during transient flow at engine ignition and staging. For example, an upper-stage nozzle may be required to start before stage separation and fire into an inadequately vented space. The ambient pressure would then rise, and the nozzle would operate overexpanded until stage separation occurred.

The purpose of this study is to explore briefly the mechanism of the aeroelastic instabilities of an overexpanded rocket nozzle. Lightweight nozzle extensions were tested with zero external-flow velocity. The extensions were attached to a rigid nozzle having an expansion half-angle of 22.5°. Two different area ratios were used, 54 and 100. The nozzles were mounted in the wall of a Langley Research Center vacuum chamber, and experiments were carried out for ratios of stagnation pressure to ambient pressure up to 15 000 with atmospheric stagnation pressure.

No attempt was made to scale any particular configuration, and the test conditions did not simulate actual flight conditions, except for the starting ambient pressure, which was equivalent to an altitude of 225 000 feet (69 000 meters). The stagnation pressure was an order of magnitude less than that of actual rocket combustion-chamber pressures, and there was no external flow over the nozzle extension. The test method of operation was analogous to "diving" an actual rocket engine; that is, the ambient pressure increased during a model test run.

SYMBOLS

E	Young's modulus
l	slant length of cone
$\dot{m}$	mass-flow rate through nozzle
p	vacuum-chamber pressure
p_o	initial vacuum-chamber pressure
R	gas constant
r_1	small-end radius
r_2	large-end radius
T	temperature
t	shell thickness
V	vacuum-chamber volume

α cone half-angle

$\rho = \frac{r_1 + r_2}{2 \cos \alpha}$

τ time

APPARATUS AND PROCEDURE

The experimental apparatus was mounted through the wall of the 55-foot-diameter, 55-foot-high (16.8-meter-diameter, 16.8-meter-high) cylindrical vacuum tank at the Langley Research Center. This tank has a volume of 135 000 cubic feet (3820 cubic meters). With mechanical pumps the chamber was evacuated to about 5×10^{-2} torr (6.67 newtons/meters^2), which is equivalent to a pressure altitude of 225 000 feet (68 600 meters).

Models

Figure 1 shows a sketch of the nozzle and nozzle extensions, and photographs of one configuration are shown in figure 2. The rigid conical nozzle had a 3-inch-diameter (7.6-centimeter) throat, a 12.0-inch-diameter (30.5-centimeter) exit, and a 22.5° expansion half-angle. Flow through the nozzle was started and stopped in the nozzle throat by a plug valve that could be pulled out beyond the entrance cone to allow free flow.

Two sizes of flexible nozzle extensions were used. One had a 22-inch (55.9-centimeter) exit diameter (short extension) and the other had a 30-inch (76.2-centimeter) exit diameter (long extension). Some physical properties of the flexible extensions are given in table I. The glass-fiber-reinforced laminates were built up with 0.004-inch-thick (0.102-millimeter) satin-weave cloth, cross laminated and vacuum molded with a polyester resin.

Instrumentation

Pressures were measured on rigid nozzle extensions that were similar in geometry to the flexible extensions and constructed from 1/4-inch-thick (0.64-centimeter) aluminum alloy. Figure 1 shows the location of the pressure orifices. Thermopile pressure gages having relatively slow response times (approximately 2 seconds) were used to measure the steady-state pressures, while variable-reluctance gages with very rapid response times were used to detect any unsteady pressures. These gages could detect pressure fluctuation of about 0.52 torr (69.3 newtons/meters^2) and the response of the recording system was flat to 100 hertz. A McLeod gage was used to measure the vacuum-chamber pressure.

Several flow-visualization techniques were used during the investigation. A double-pass schlieren system was used with a 400-frames-per-second camera. The light beam looked across the lower half of the exit flow as shown in figure 3. Tufts were mounted on wires that spanned the extension exit to indicate the progression of the separated flow across the exit. Tufts glued to the inside of the extension surface (not shown in fig. 3) indicated the progression of the separated flow as it moved upstream. The tests were also documented by motion pictures taken at 400 frames per second.

Test Procedure

With the model installed and the throat valve in place, the 55-foot (16.8 meter) vacuum chamber was evacuated to about 5×10^{-2} torr (6.67 newtons/meter^2). At this ambient pressure and at atmospheric stagnation pressure, flow would start in an underexpanded condition in the extensions of either length. These tests were run at stagnation pressures one order of magnitude less than operational rockets use. A few seconds before the throat plug valve was opened, all the recording equipment was started. The valve was then opened for the length of time needed to complete the particular test. For pressure surveys, 30 seconds was long enough for the overexpanded nozzle condition to force separation of flow well upstream of the extension exit. For the aeroelastic tests, the run time was determined by the behavior of the model: When instability occurred the test was stopped; if no instability was encountered, the test continued until flow separation was well upstream of the exit.

RESULTS AND DISCUSSION

Rigid-Extension Pressure-Distribution Tests

The results of the pressure measurements on the long rigid extensions are shown in figures 4 to 6. Figure 4 shows the variation of the vacuum-chamber pressure and the wall pressures along the inside of the long extension with time. Over the range of these tests, the vacuum-chamber pressure follows the equation

$$p = p_o + \frac{\dot{m}RT\tau}{V}$$

The orifice pressures remain constant until separation occurs, and then the pressure begins to rise at about the same rate as the rise in chamber pressure. Figure 4 shows the upstream progression of the separated flow as the vacuum-chamber pressure increases. The shock wave off the separated flow can be seen in the schlieren pictures of figure 5, and the tufts show the region of reversed flow. Although the schlieren motion pictures showed that the shock waves were unsteady, no unsteady pressures were recorded by the high-frequency-response pressure gages. Figure 6 shows the measured

and calculated one-dimensional pressure distribution along the length of the wall of the long extension at various times. No discontinuous pressure rise (as would be expected from inviscid-flow theory) was measured at any of the orifices as the separated flow moved upstream. Tufts glued to the inside of the extensions showed very erratic behavior once separation had occurred; however, no pressure fluctuations were detected.

Flexible-Extension Tests

Three of the flexible extensions tested were unstable: two long extensions with thicknesses of 0.014 and 0.0095 inch (0.356 and 0.241 millimeter) and one short extension with a thickness of 0.0095 inch (0.241 millimeter). All three were constructed of glass-fiber laminates. Some physical properties of these and also of two stable extensions are listed in table I.

The mechanism of collapse of the unstable extensions was studied by observing high-speed motion pictures taken during the tests. The aeroelastic instability of both the long and the short extensions started with slight buckling at the free end of the extension. The buckling progressed toward the small end of the extension with no dynamic instability until buckling deflections of large amplitude (1 to 2 inches (25.4 to 50.8 millimeters)) had developed. The dynamic instability was an erratic oscillation that roughly resembled a standing wave having the buckled mode shape. As soon as dynamic instability occurred, the test was stopped to avoid destruction of the model. Figures 7 and 8 are enlargements of 16-millimeter high-speed motion-picture frames showing the development of the instabilities from very small to maximum-amplitude deflections.

In an attempt to induce dynamic instability the natural frequency of one of the unstable extensions was reduced by a factor of 1.7 by the addition of small lead weights which did not increase the stiffness. This large change in frequency had no effect on the instability. The addition of the weights did, however, lower the average pressure loading at which buckling occurred. The reduction in pressure loading was equivalent to the loading due to the weights. Motion pictures of the test showed that in this case buckling started on the upper part of the extension where the weights acted as a compressive load.

The net pressure distribution over the external wall of extensions A to E is shown in figure 9. The pressure distribution at the onset of buckling is shown for the unstable extensions (A, B, and D) and the distribution at the time of maximum loading for the stable cases (C and E). Since buckling started at the free end of the extension (as observed in the high-speed movies), the buckling load is arbitrarily defined as the average external pressure over the downstream half of the extension (stations 1 to 4 for the short extension and 1 to 6 for the long extension).

The experimental results are summarized graphically in figure 10, in which the arbitrarily defined buckling load for the stable and unstable extensions is plotted as a function of an empirical buckling parameter (ref. 2) defined as

$$\text{Buckling parameter} = \frac{E}{\frac{l}{\rho}\left(\frac{\rho}{t}\right)^{5/2}}$$

The results presented in figure 10 indicate the stable and unstable regions for different pressure loadings and physical parameters of the extensions. The limited amount of data, however, prohibits establishing a well-defined boundary between the stable and the unstable areas. The stability boundary is, therefore, indicated by the shaded region. The results in figure 10 are presented only as a rough indication of stable extension parameters which may be used as a guide in preliminary design.

CONCLUDING REMARKS

A brief exploratory investigation has been made to study possible aeroelastic-instability phenomena which might occur for flexible rocket nozzle extensions. The study was limited to conditions with no external flow over the extensions.

On the basis of the test results, dynamic instability of overexpanded nozzle extensions is apparently caused by aerodynamic forces resulting from buckling. There was no evidence that initial instability was a forced or self-excited phenomenon; consequently, the design problem should be simplified since a dynamic analysis is not required.

The experimental data are summarized graphically to indicate nozzle-extension parameters in the stable region for different loading conditions. The results may be useful as a guide in the preliminary design of extensions.

Langley Research Center,
National Aeronautics and Space Administration,
Langley Station, Hampton, Va., December 18, 1967,
124-08-05-09-23.

REFERENCES

1. Sutton, George P.: Rocket Propulsion Elements. John Wiley & Sons, Inc., 1949.

2. Seide, P.; Weingarten, V. I.; and Morgan, E. J.: The Development of Design Criteria for Elastic Stability of Thin Shell Structures. AFBMD/TR-61-7, U.S. Air Force, Dec. 31, 1960.

TABLE I.- NOZZLE-EXTENSION PROPERTIES AND TEST RESULTS

Extension	Area ratio	Material	Thickness		Young's modulus[a]		Test results
			in.	mm	psi	N/m^2	
A	100	Fiber glass	0.014	0.356	1.33×10^6	9.17×10^9	Unstable
B	100	Fiber glass	.0095	.241	1.17	8.07×10^9	Unstable
C	100	Steel	.0070	.178	29	2.00×10^{11}	Stable
D	54	Fiber glass	.0095	.241	1.71	1.18×10^{10}	Unstable
E	54	Fiber glass	.0135	.343	1.45	1.0×10^{10}	Stable

[a]Young's modulus for the fiber-glass-reinforced plastic was measured after testing on four samples from each extension. Values ranged ±25 percent about the average values listed.

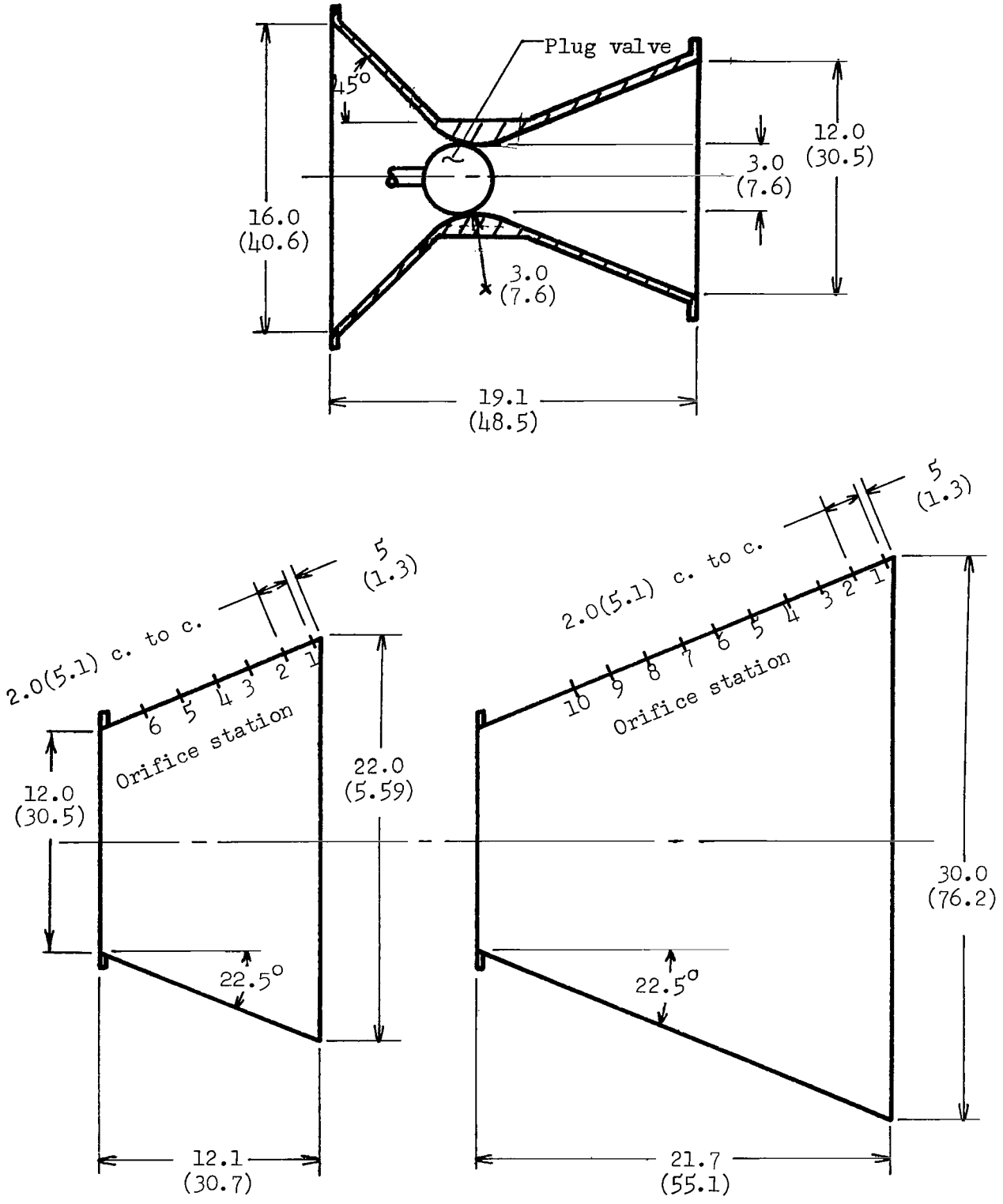

Figure 1.- Sketch of rigid nozzle and rigid nozzle extensions. Flexible extensions had similar geometry but no orifices. Dimensions in inches (centimeters).

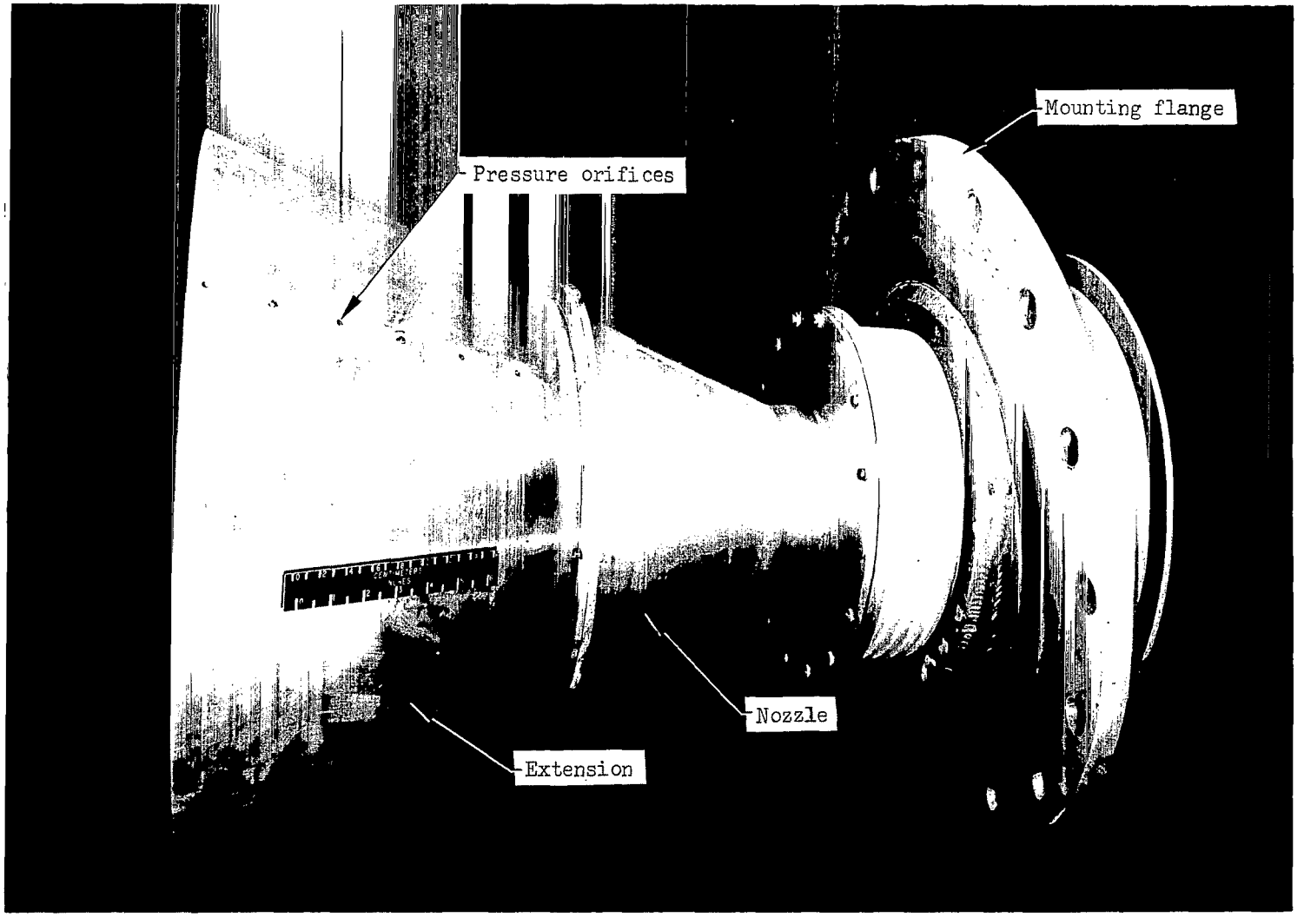

(a) Nozzle and extension. L-66-9993.1

Figure 2.- Nozzle and short rigid extension used for pressure measurements.

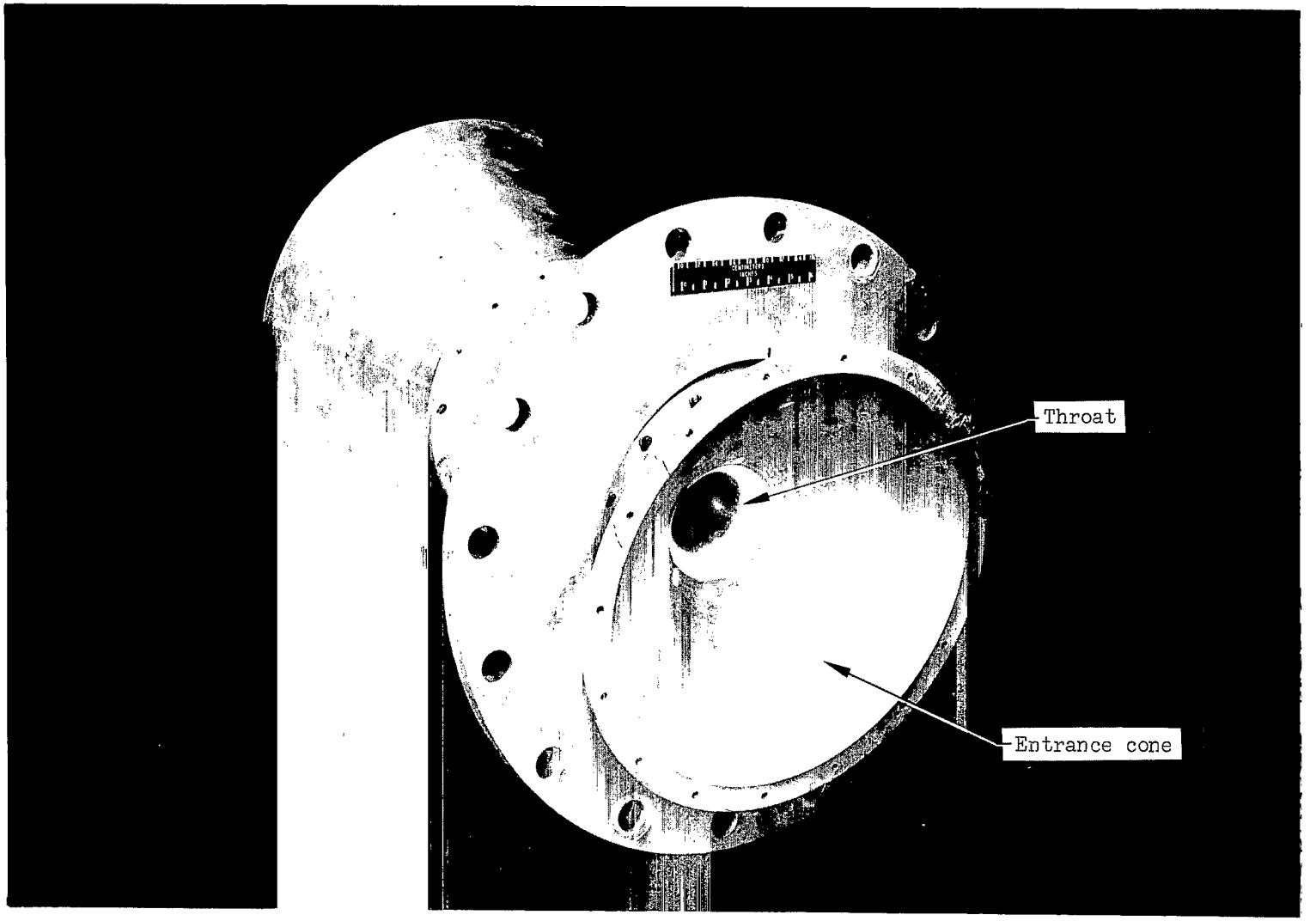

(b) Nozzle entrance cone. L-66-9992.1

Figure 2.- Concluded.

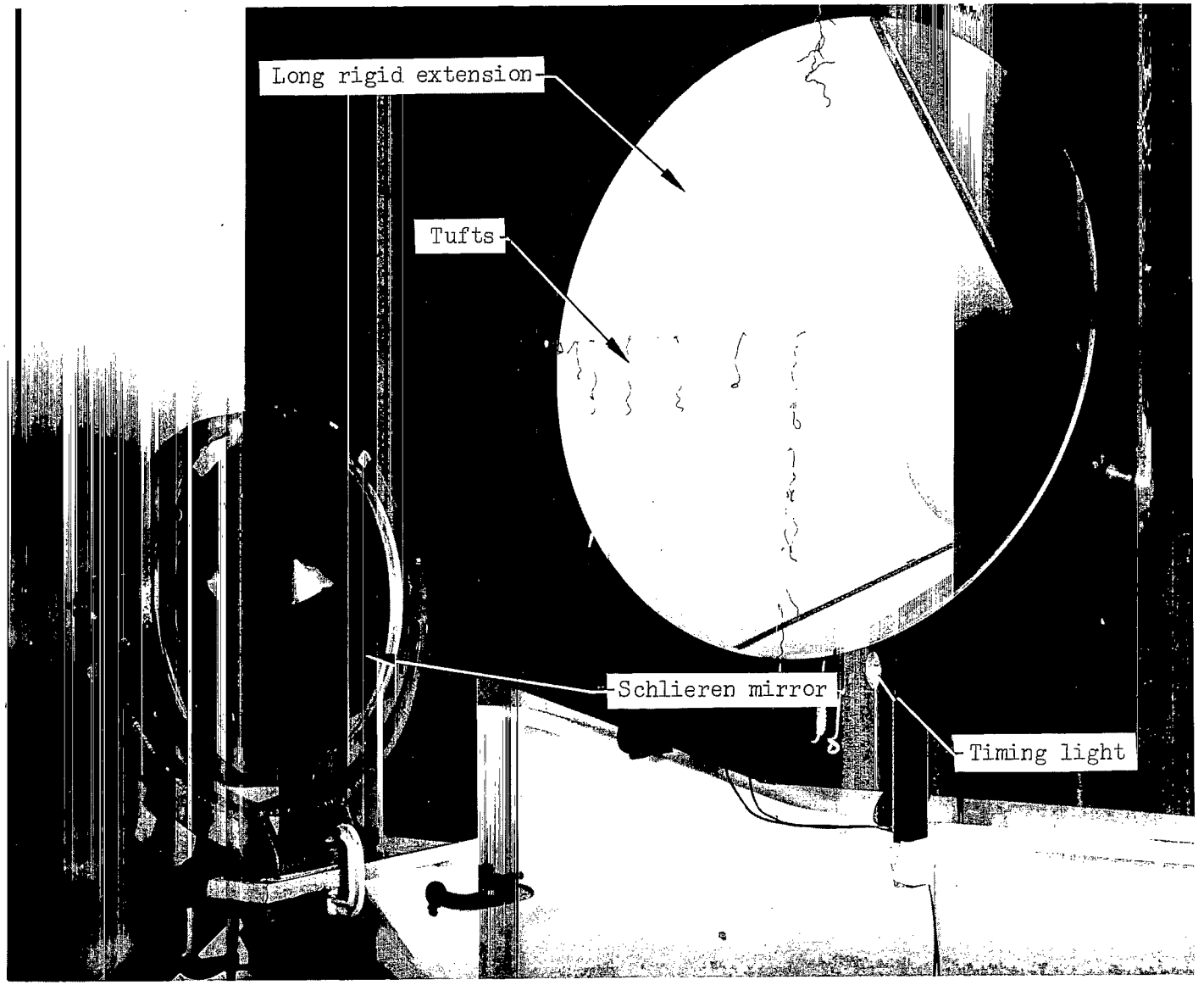

Figure 3.- Flow visualization arrangement. L-68-801

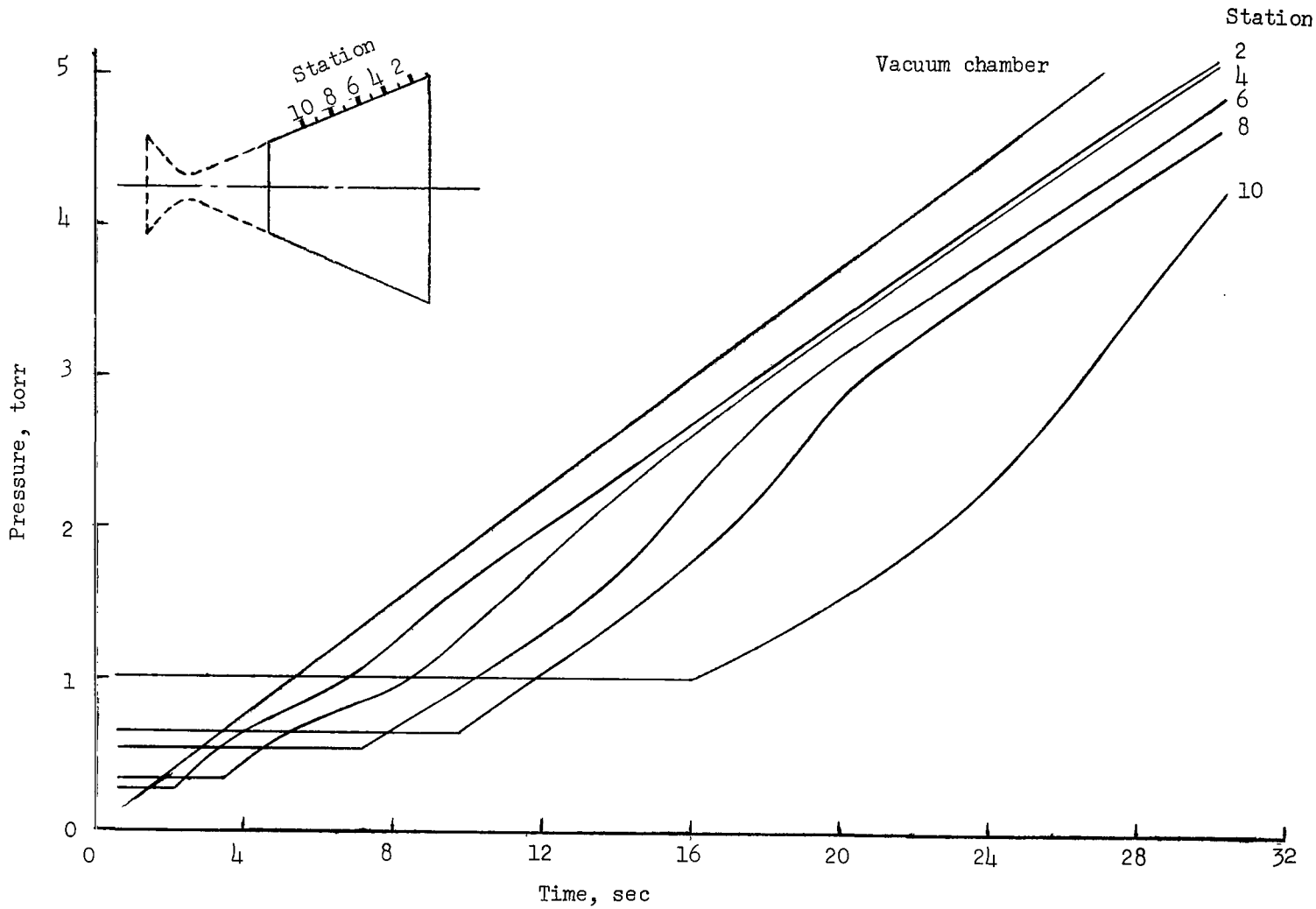

Figure 4.- Pressure variation with time at several stations on long extension.

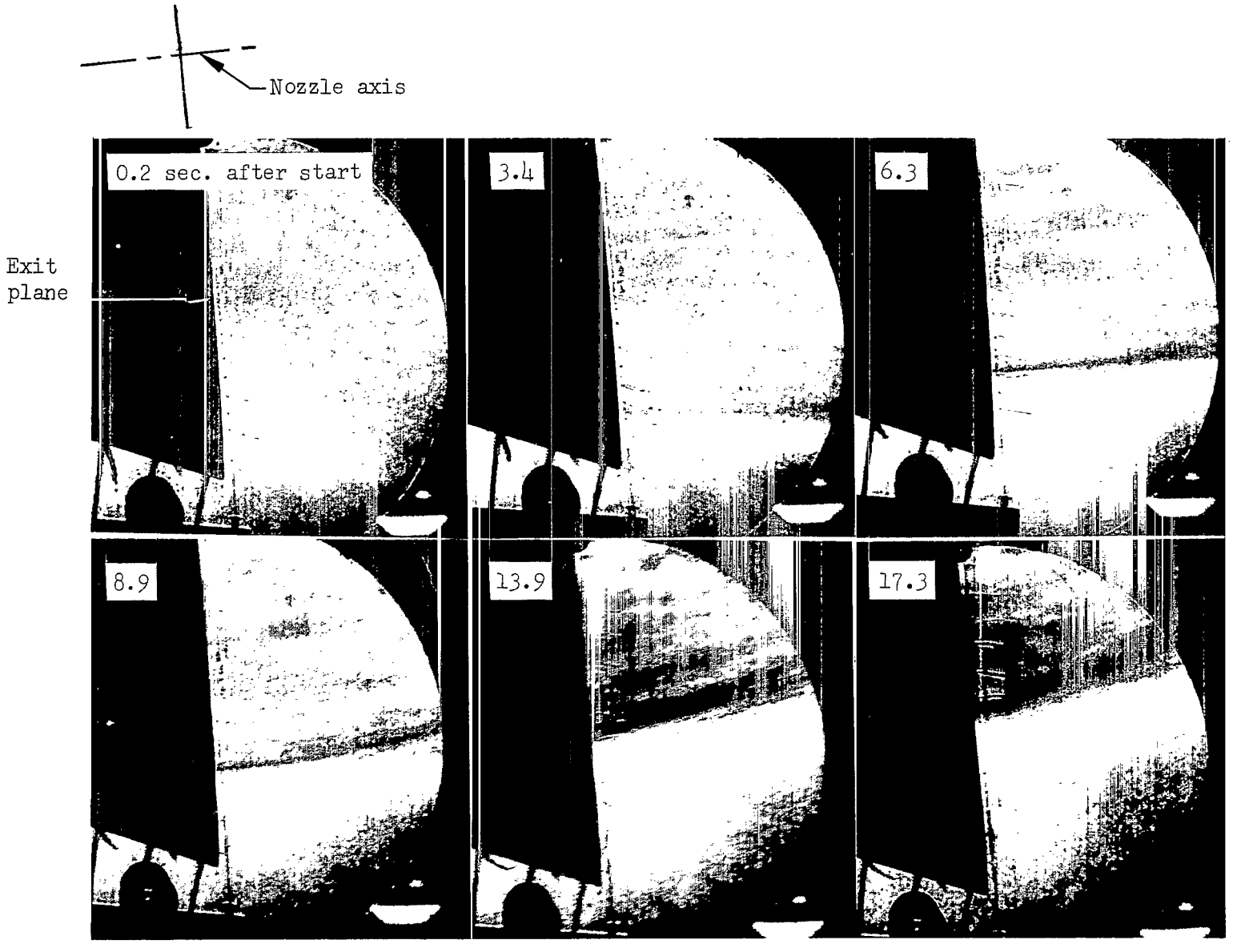

Figure 5.- Flow-visualization pictures (schlieren and tufts) of long rigid extension. L-68-802

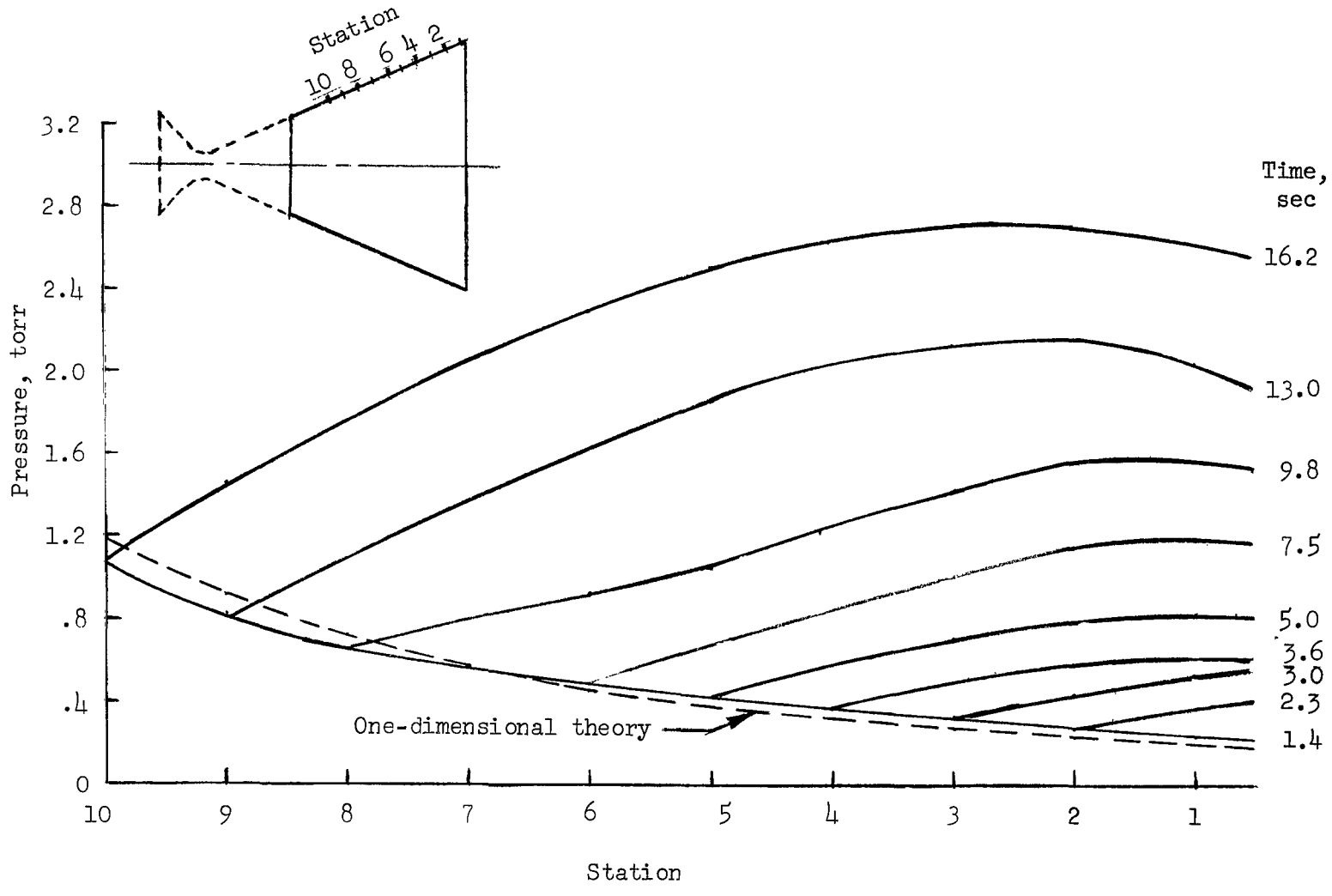

Figure 6.- Pressure distribution on long extension at various times.

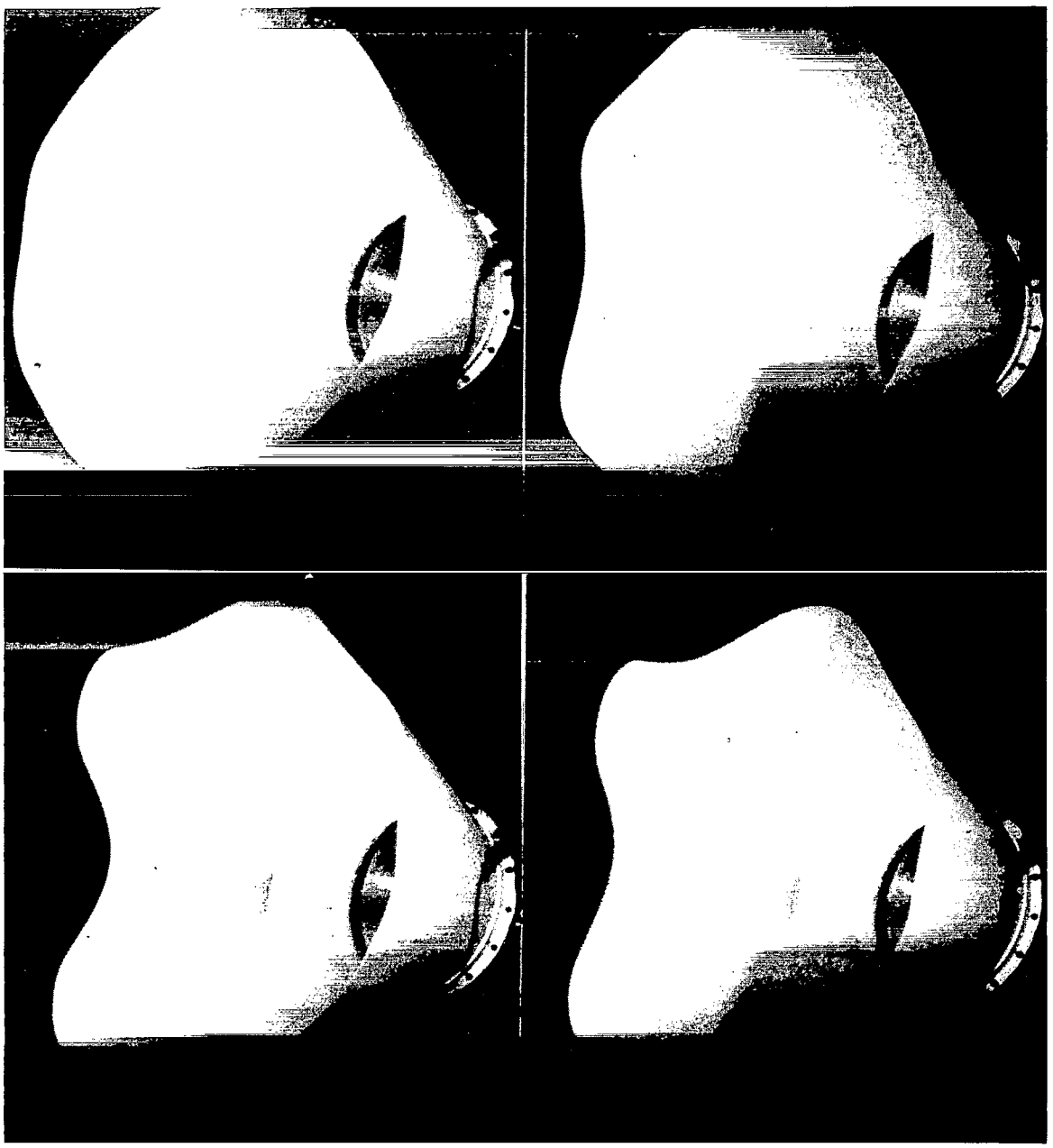

Figure 7.- Instability mode of long glass-fiber extension, 0.014 inch (0.356 millimeter) thick. L-68-803

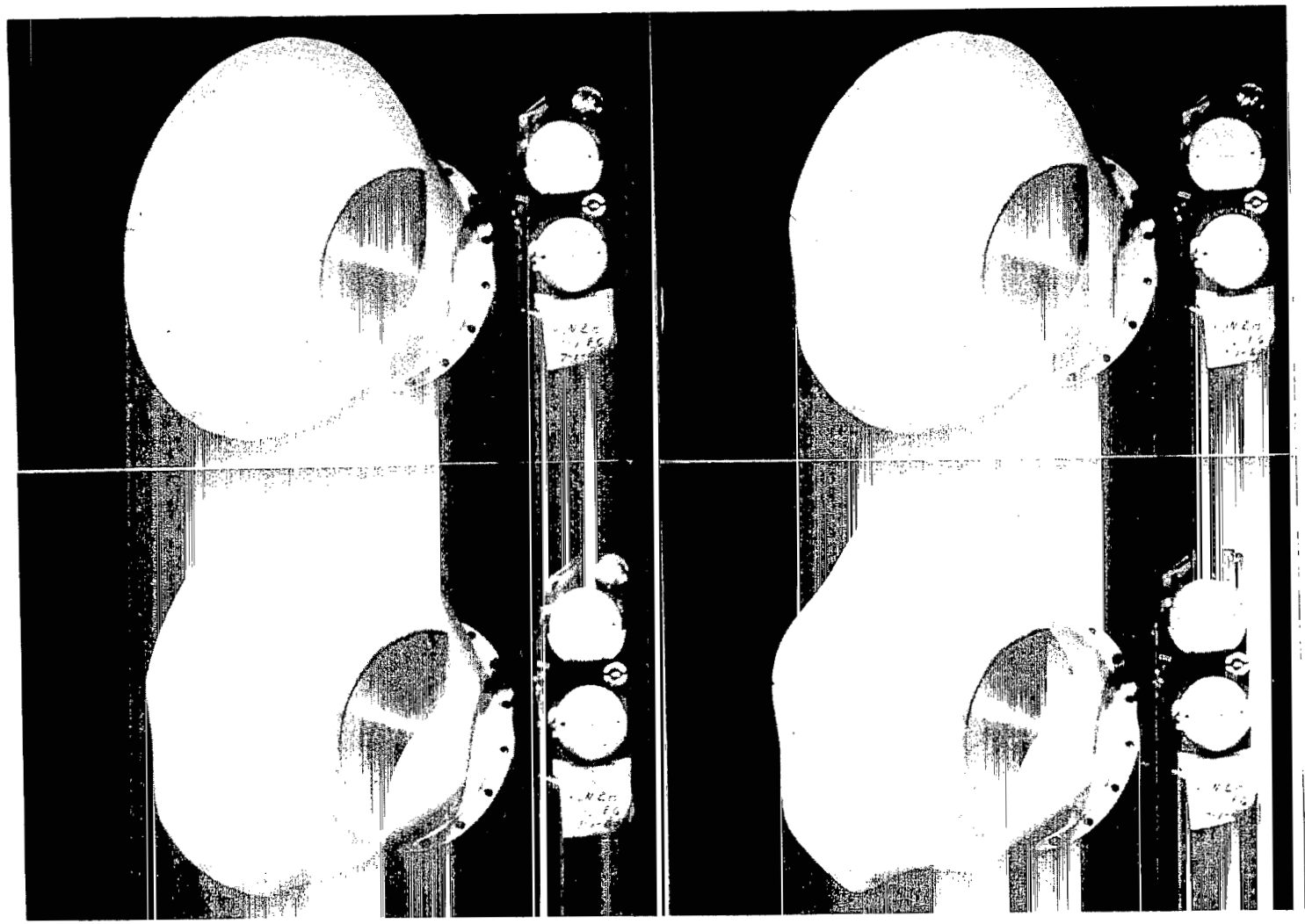

Figure 8.- Instability mode of short glass-fiber extension, 0.0095 inch (0.241 millimeter) thick. L-68-804

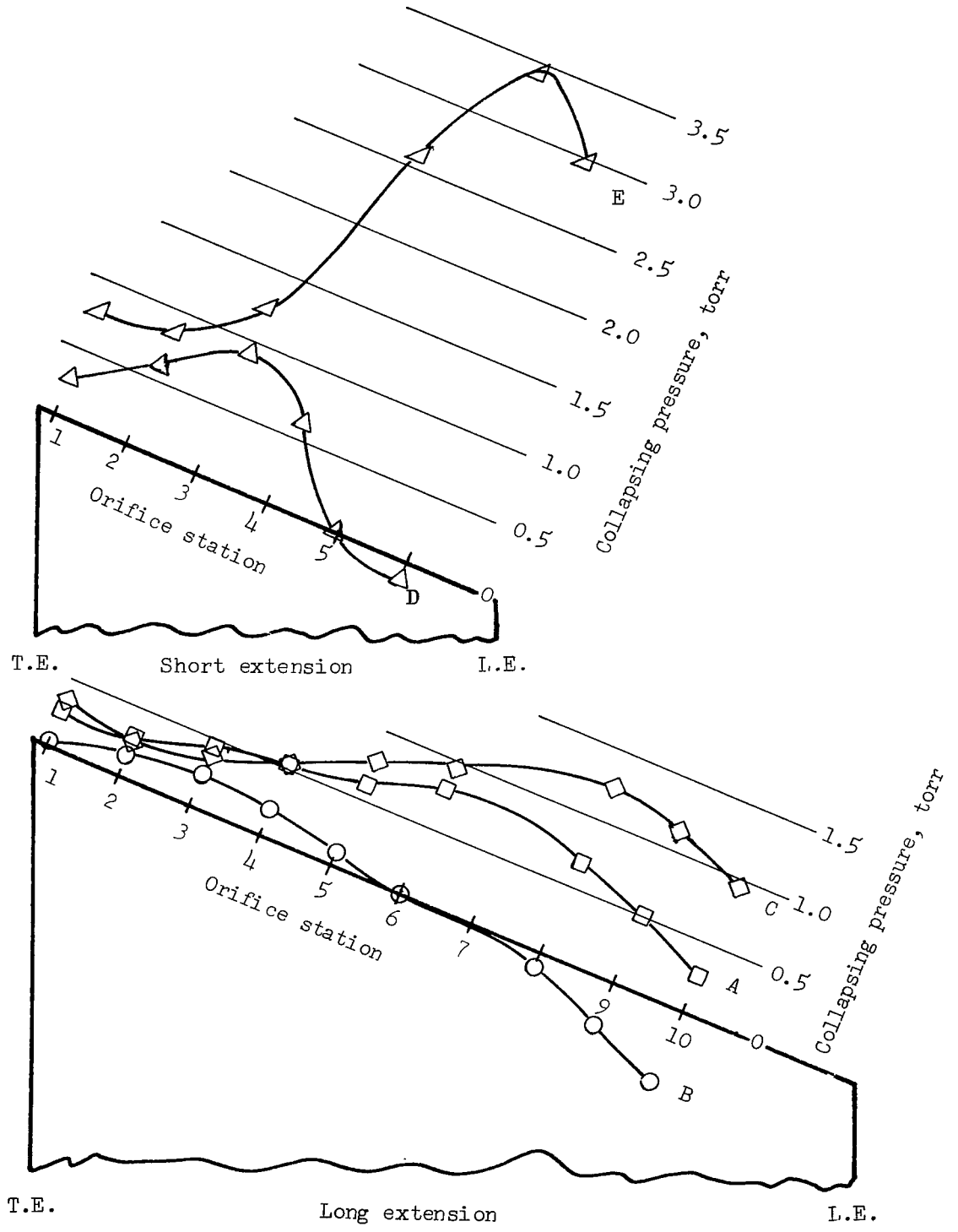

Figure 9.- Pressure distributions over extensions at the time of buckling or at maximum loading.

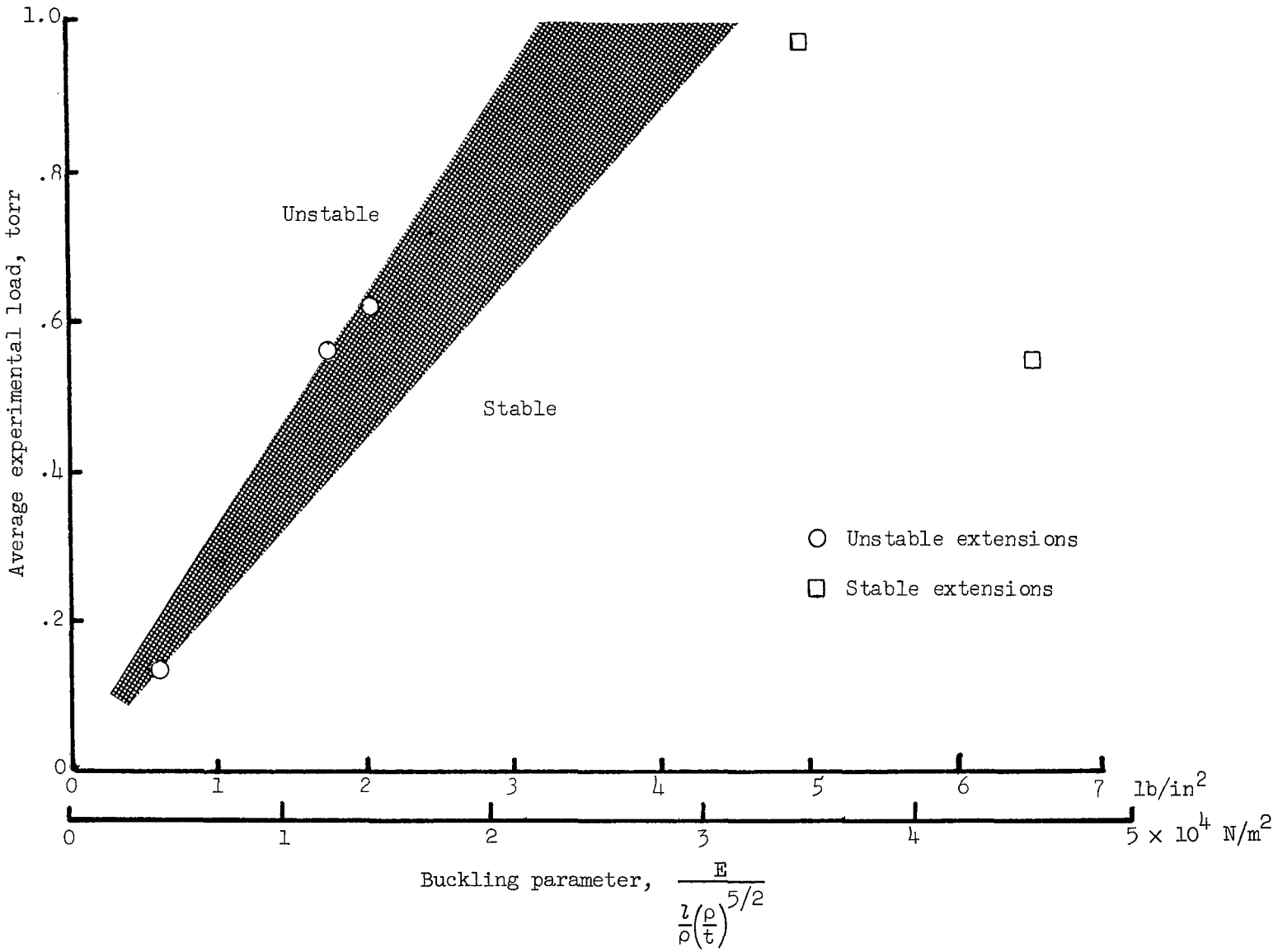

Figure 10.- Average experimental loading over downstream half of extension at buckling or maximum loading, compared with an empirical buckling parameter.

"The aeronautical and space activities of the United States shall be conducted so as to contribute . . . to the expansion of human knowledge of phenomena in the atmosphere and space. The Administration shall provide for the widest practicable and appropriate dissemination of information concerning its activities and the results thereof."

—NATIONAL AERONAUTICS AND SPACE ACT OF 1958

NASA SCIENTIFIC AND TECHNICAL PUBLICATIONS

TECHNICAL REPORTS: Scientific and technical information considered important, complete, and a lasting contribution to existing knowledge.

TECHNICAL NOTES: Information less broad in scope but nevertheless of importance as a contribution to existing knowledge.

TECHNICAL MEMORANDUMS: Information receiving limited distribution because of preliminary data, security classification, or other reasons.

CONTRACTOR REPORTS: Scientific and technical information generated under a NASA contract or grant and considered an important contribution to existing knowledge.

TECHNICAL TRANSLATIONS: Information published in a foreign language considered to merit NASA distribution in English.

SPECIAL PUBLICATIONS: Information derived from or of value to NASA activities. Publications include conference proceedings, monographs, data compilations, handbooks, sourcebooks, and special bibliographies.

TECHNOLOGY UTILIZATION PUBLICATIONS: Information on technology used by NASA that may be of particular interest in commercial and other non-aerospace applications. Publications include Tech Briefs, Technology Utilization Reports and Notes, and Technology Surveys.

Details on the availability of these publications may be obtained from:

SCIENTIFIC AND TECHNICAL INFORMATION DIVISION

NATIONAL AERONAUTICS AND SPACE ADMINISTRATION

Washington, D.C. 20546